

The Shaping of the Multipolar Pre-Planetary Nebula CRL 618 by Multi-directional Bullets

Po-Sheng Huang^{1,2}, Chin-Fei Lee^{1,2}, Anthony Moraghan¹, and Michael Smith³

Received _____; accepted _____

¹Academia Sinica Institute of Astronomy and Astrophysics, P.O. Box 23-141, Taipei 106, Taiwan; posheng@asiaa.sinica.edu.tw

²Institute of Astrophysics, National Taiwan University, Taipei 106, Taiwan

³Centre for Astrophysics and Space Science, University of Kent, Canterbury CT2 7NH, UK

ABSTRACT

In order to understand the formation of the multipolar structures of the pre-planetary nebula (PPN) CRL 618, we perform 3D simulations using a multi-directional bullet model. The optical lobes of CRL 618 and fast molecular outflows at the tips of the lobes have been found to have similar expansion ages of ~ 100 yr. Additional fast molecular outflows were found near the source along the outflow axes with ages of ~ 45 yr, suggesting a second episode of bullet ejections. Thus, in our simulations, two episodes of bullet ejections are assumed. The shaping process is simulated using the ZEUS-3D hydrodynamics code that includes molecular and atomic cooling. In addition, molecular chemistry is also included to calculate the CO intensity maps. Our results show the following: (1) Multi-epoch bullets interacting with the toroidal dense core can produce the collimated multiple lobes as seen in CRL 618. The total mass of the bullets is $\sim 0.034 M_{\odot}$, consistent with the observed high-velocity CO emission in fast molecular outflows. (2) The simulated CO $J = 3-2$ intensity maps show that the low-velocity cavity wall and the high-velocity outflows along the lobes are reasonably consistent with the observations. The position-velocity diagram of the outflows along the outflow axes shows a linear increase of velocity with distance, similar to the observations. The ejections of these bullets could be due to magneto-rotational explosions or nova-like explosions around a binary companion.

Subject headings: planetary nebulae: general — stars: AGB and post-AGB — stars: mass-loss — stars: winds, outflows

1. INTRODUCTION

Pre-planetary nebulae (PPNe) are transient objects between the asymptotic giant branch (AGB) phase and the planetary nebula (PN) phase in the evolution of low- to intermediate-mass stars. In less than a thousand years, PPNe will transform into PNe when the central stars evolve to hot white dwarfs and photoionize their envelopes. Most PPNe are aspherical and found to possess bipolar or multipolar lobes (Corradi & Schwarz 1995; Sahai 2001; Sahai et al. 2007) with kinematic ages less than 1000 yr (Bujarrabal et al. 2001). Bipolar lobes can be produced by fast winds ejected from around central stars near the end of the AGB phase. However, multipolar PPNe may not be produced in the same way, because the fast winds, even if precessing, have difficulty producing the multipolar morphology.

CRL 618 is one of the most well-studied multipolar PPNe, and thus a good candidate for our study of the mass-loss process in multipolar PPNe. In the *Hubble Space Telescope* (*HST*) images, multipolar optical lobes were observed in the east-west direction (Trammell & Goodrich 2002). These optical lobes are expanding rapidly away from the center (Sánchez Contreras et al. 2002). Infrared observations in H_2 (Cox et al. 2003), and (sub)millimeter observations in CO $J = 2-1$ (Sánchez Contreras et al. 2004), $J = 3-2$ (Lee et al. 2013a,b), and $J = 6-5$ (Nakashima et al. 2007) revealed fast molecular outflows along the optical lobes. A dense core was detected around the central star (Lee et al. 2013a) surrounded by a tenuous spherical halo (Sánchez Contreras et al. 2004).

Two-dimensional hydrodynamical simulations have attempted to reproduce the lobe morphology of CRL 618. Lee & Sahai (2003) and Lee et al. (2009) used a collimated fast wind (CFW) model to produce one of the well-defined lobes in the west by using the ZEUS-2D hydrodynamics code. In the CFW model, the PPN lobes are a result from the interaction of the fast winds with the surrounding AGB halo. The CFW can reproduce the

structures and kinematics of the outflow lobe. However, the CFW may need to be more confined like a cylindrical jet in order to produce enough shock emission.

On the other hand, Dennis et al. (2008) showed that a massive clump (bullet) model can also produce the structure and kinematics of a lobe in CRL 618. Recently, Balick et al. (2013) measured proper motions of the optical lobes and found that the fingertips of the lobes have the same expansion ages of $\sim 100\pm 15$ yr. Therefore, these optical lobes likely all resulted from a spray of bullets in different directions. As a result, Balick et al. (2013) followed up with the bullet model and included the periodical density enhancement in the AGB halo in order to produce the observed ringlike structures in the lobe.

Later, the fast molecular outflows at the tips of the optical lobes are also found to have similar expansion ages to the optical lobes (Lee et al. 2013b). This suggests that the optical lobes and the fast molecular outflows likely all resulted from the same spray of bullets. Additional fast molecular outflows are found near the source along the outflow axes with ages of $\sim 45\pm 25$ yr, suggesting a second episode of bullet ejections. But the origin of the bullets is still unknown. The bullet ejections could be due to magneto-rotational explosions (Matt et al. 2006) or nova-like explosions (Lee et al. 2013a).

More recently, Riera et al. (2014) adopted a precessing jet model (Velázquez et al. 2012, 2013) to reproduce the multipolar morphology of CRL 618. If the jet source is also pulsing and the precession period is an integer multiple of the pulsing period, the jet can produce multiple lobes. But this model can only produce point-symmetric lobes. In order to reproduce the asymmetric lobes as seen in CRL 618, a complicated “asymmetrical jet ejection mechanism” (Montgomery 2012) is required (Velázquez et al. 2014).

In this paper, in order to understand the formation of the multipolar structures of CRL 618, we perform 3D simulations using a multi-directional bullet model. Unlike previous bullet models, our AGB halo has parameters close to those derived from the observations of

CRL 618. In addition, a dense core around the center is also included, as in the observations. The inclusion of the dense core is important to derive the masses of the bullets accurately, because the resulting velocity of the bullets depends on the interactions of the bullets with the dense core. For the first attempt, we only model the lobes in the east of CRL 618. As suggested in Lee et al. (2013b), two episodes of bullet ejections are assumed, first with two bullets to produce the two major lobes, and second with three bullets to produce the fast molecular outflows near the source. The numerical settings and assumptions are given in section 2; we compare the 3D simulations and simulated CO intensity maps with observations in section 3; in section 4 we discuss the results and possible origin of bullets; and we summarize this work in section 5.

2. NUMERICAL SETTINGS

We perform the simulations of the bullet model using the ZEUS-3D code, which is a grid-based computational fluid dynamics code (Clarke 1996, 2010). The code has been expanded to include molecular and atomic cooling by Suttner et al. (1997). In addition, molecular chemistry is also included to calculate the fraction of molecular hydrogen and atomic hydrogen (Smith & Rosen 2003). The material is assumed to consist of mostly molecular hydrogen. Helium is also included with the number density $n_{\text{He}} = 0.1n_{\text{H}}$, where n_{H} is the number density of the hydrogen nuclei. The CO-to-H₂ relative abundance is assumed to be 2×10^{-4} , as adopted in Sánchez Contreras et al. (2004).

In our simulations, a Cartesian coordinate system is used. The x -axis is the polar axis. The y - and z -axes are in the equatorial plane, perpendicular to the polar axis. We use $576 \times 400 \times 400$ cells with a resolution of 12.5 AU per cell to cover from 0 to 7200 AU in the x -axis, -2500 to 2500 AU in the y -axis, and -2500 to 2500 AU in the z -axis. We adopt a distance $D = 900$ pc for CRL 618 (Sánchez Contreras & Sahai 2004). The resolution of

12.5 AU corresponds to an angular resolution $\sim 0''.014$, high enough to show the details of the lobes and the outflows to be compared with the *HST* (e.g., up to $0''.07$ in Balick et al. 2013) and SMA observations (e.g., up to $0''.5$ in Lee et al. 2013a) of CRL 618.

In our simulations, a number of bullets are ejected from the central source, interacting with the surrounding to produce the multipolar lobes. The surrounding consists of an AGB halo with a dense core at the center.

2.1. Bullets

Figure 1a shows the optical lobes of CRL 618 in the $H\alpha$ image, taken by the *HST* in 2009 August. The outflow lobes labeled with E1, E2 and E3 are clearly detected in optical. The labels E4 and E5 indicate the positions of the two molecular outflow lobes detected in the high-velocity CO emission map (Lee et al. 2013b), as shown in Figure 1b. In our models, bullets are used to produce the optical lobes and the fast molecular outflows along the lobes. According to the observations (Lee et al. 2013b), there would be two episodes of bullet ejections. In Model 1, two bullets (bullets 1 and 2) are ejected from the central source in the first episode at a simulation time of ~ 90 yr ago in order to produce the two major lobes, E1 and E2, in the east of CRL 618. In order to avoid the collision between the two bullets, the second bullet is ejected 6 yr after the first bullet. In Model 2, we add a second episode of three bullets (bullets 3, 4, and 5) at ~ 40 yr after the first episode, in order to produce the additional fast outflows (lobes E3, E4, and E5) near the source in the east of CRL 618. Again, in order to avoid the collision between the bullets, we assume that bullets 3, 4, and 5 are ejected one by one with a time delay of 6 yr. Notice that lobe E3 was assumed to have a similar dynamical age to lobes E1 and E2 in Balick et al. (2013). Here it is assumed to have a similar dynamical age to lobes E4 and E5, as in Lee et al. (2013b). This assumption is reasonable because lobe E3 has a similar length and radial velocity to

lobe E5.

All the bullets are assumed to be ejected from the center. They are cylindrical with a diameter $d_b = 200$ AU and a length $l_b = 200$ AU. In the observations of CRL 618 by Sánchez Contreras et al. (2004), most of the gas in the fast outflows are at temperatures of ~ 200 K. Therefore, we set the temperature of the bullets to 200 K.

The ejection velocities of the bullets in CRL 618 are unknown, but their lower limits can be estimated from the transverse velocities (proper motions) of the optical lobes, v_t (Riera et al. 2014) and the radial velocities of the fast outflows, v_r (Lee et al. 2013b). Table 1 shows the lower limits calculated with $v = (v_t^2 + v_r^2)^{1/2}$. The ejection velocities v_b must be higher than the lower limits but not by much, because the bullets are much denser than the surrounding. Therefore, in our simulations, we set the ejection velocities to be slightly higher. As shown in Table 2, the ejection velocities v_b are 330 and 350 km s⁻¹ for bullets 1 and 2, 280 km s⁻¹ for bullet 3, and 240 km s⁻¹ for bullets 4 and 5.

The ejection orientation of the bullets is defined by the position angle, θ_p , and the inclination angle, $\theta_i = \tan^{-1}(v_r/v_t)$, of the outflow axis of the optical lobes and fast outflows, as listed in Table 1. For example, we assume bullet 1 to be ejected along the outflow axis of lobe E1 which has $\theta_p = 90^\circ$ and $\theta_i = -24^\circ$ (Fig. 2). This axis is also set to be the x -axis in our simulations. Since no fast outflow was observed at the tip of lobe E2, the inclination angle of lobe E2 can not be determined. Lobe E2 is assumed to have $\theta_i = -32^\circ$, lying slightly in front of lobe E1. The inclination angle of lobes E4 and E5 are set to -35° and -45° , similar to the observed values. For lobe E3, the transverse velocity and thus the inclination angle are uncertain. We set $\theta_i = -45^\circ$ for this lobe, like lobe E5.

The bullet mass is set to $\sim 0.011 M_\odot$ for bullets 1 and 2, and $0.004 M_\odot$ for bullets 3, 4, and 5. The total mass of the bullets is therefore $\sim 0.034 M_\odot$. This value is about half of the total mass ($0.065 M_\odot$) estimated from the total flux of the fast molecular outflows

in the east and west of CRL 618 (with $|v| > 20 \text{ km s}^{-1}$, Lee et al. 2013b). Therefore, this value is consistent with the observations. The density of the bullets is given by

$$\rho_b = \frac{M_b}{\pi(d_b/2)^2 l_b} \quad (1)$$

where d_b , l_b , and M_b are the diameter, length, and mass of the bullets. As mentioned earlier, d_b and l_b are both 200 AU. Therefore, the density of the bullets is $\sim (0.4\text{--}1.0) \times 10^{-15} \text{ g cm}^{-3}$, and thus the number density of hydrogen nuclei in the bullets is $\rho_b/(1.4m_{\text{H}}) \sim (1.6\text{--}4.4) \times 10^8 \text{ cm}^{-3}$ (Table 2).

In our model, the densities of the bullets are higher than those adopted in the previous simulations: Balick et al. (2013) adopted a number density of $4 \times 10^4 \text{ cm}^{-3}$ for the bullet in their model. Unlike their model, there is a dense core present in our model. Riera et al. (2014) and Velázquez et al. (2014) adopted an average density of 10^6 cm^{-3} for the jet in their precessing jet model. In their model, a dense core is included, with a density of $\sim 10^6 \text{ cm}^{-3}$ near the source. In our model, the dense core has a density of $\sim 10^8 \text{ cm}^{-3}$ near the source (as described in the next section), which is ~ 2 orders of magnitude higher than that in their precessing jet model. Thus, higher-density bullets are needed to excavate the holes in the dense core. As discussed earlier, the total mass of the bullets is $0.034 M_{\odot}$, still consistent with the submillimeter observations.

The mass-loss rate is given by

$$\dot{M}_b = \pi \left(\frac{d_b}{2}\right)^2 v_b \rho_b, \quad (2)$$

which is $\sim 4 \times 10^{-3} M_{\odot} \text{ yr}^{-1}$ for bullets 1 and 2, and $\sim 10^{-3} M_{\odot} \text{ yr}^{-1}$ for bullets 3, 4, and 5.

2.2. The AGB Halo and the Dense Core

The AGB halo is assumed to be spherical symmetric with a constant mass-loss rate.

Thus, the density of the AGB halo is given by

$$\rho(r) = \frac{\dot{M}_a}{4\pi r^2 v_a} \quad (3)$$

where \dot{M}_a is the mass-loss rate assumed to be $\sim 5.5 \times 10^{-5} M_\odot \text{ yr}^{-1}$ (derived from the number density of molecular hydrogen in Table 1 in Sánchez Contreras et al. 2004, with Helium added), r is the radial distance to the central source, and v_a is the expansion velocity that was found to be $\sim 16 \text{ km s}^{-1}$ (Lee et al. 2013a). Since the bullets move much faster than the AGB halo, v_a is set to zero for simplicity, after the density of the AGB halo is calculated. In observations, the halo of CRL 618 was found to have a temperature of 10–45 K (Sánchez Contreras et al. 2004). Here we set the temperature of the AGB halo to be 10 K. These two settings of the AGB halo will not affect the dynamics of the outflow lobes to be produced.

The outer part of the dense core has been detected in CRL 618 with a radius of $\sim 1100 \text{ AU}$ (Sánchez Contreras et al. 2004). However, the actual radius of the dense core should be larger. Thus, in our simulations, the radius of the dense core R_c is assumed to be 1500 AU. The density distribution is assumed to be toroidal instead of spherical (Fig. 3) because the dense core seems to be the inner part of the expanding torus detected in the equatorial plane extending to 5000 AU from the center (Sánchez Contreras & Sahai 2004). For a toroidal density distribution, the simple form can be written as

$$\rho_c(r, \theta) = (A + B \sin^2 \theta) \rho(r), \quad \text{with } \rho(r) = \frac{\dot{M}_c(r)}{4\pi r^2 v_c(r)} \quad (4)$$

where θ is the angle measured from the polar axis, A is the isotropic parameter, and B is the toroidal parameter. The density structure would become spherical when $A = 1$ and $B = 0$. Here, for our toroidal structure, we assume $A \simeq 0.03$ and $B \simeq 2$, so that the density at $\theta = 45^\circ$ is about half of that at the equator at the same distance. $\dot{M}_c(r)$ and $v_c(r)$ are the mass-loss rate and the expansion velocity of the dense core, respectively. The density

profile in the r -axis, $\rho_c(r)$, is unknown because existing observations do not have enough resolution to resolve the dense core. Here we assume $\rho_c(r) \propto r^{-p}$. If $p = 2$ or 3 , the density at the center would become too high for the bullets to penetrate, therefore we use $p = 1$. In the observation of Lee et al. (2013a), $v_c(r)$ was found to be linearly increasing with the radius,

$$v_c(r) = \begin{cases} v_a \left(\frac{r}{r_o} \right), & \text{if } r < r_o \\ v_a, & \text{if } r_o < r < R_c \end{cases} \quad (5)$$

where $r_o = 630$ AU. After substituting $v_c(r)$ into our density profile and rearranging, we have

$$\dot{M}_c = \begin{cases} 8 \times 10^{-4} \left(\frac{r}{r_o} \right)^2 M_\odot \text{yr}^{-1}, & \text{if } r < r_o \\ 2 \times 10^{-3} \left(\frac{r}{R_c} \right) M_\odot \text{yr}^{-1}, & \text{if } r_o < r < R_c. \end{cases} \quad (6)$$

Therefore, the mass-loss rate of the dense core is ~ 40 times that of the AGB halo at $r = R_c$, and it decreases to that of the AGB halo at $r \simeq 170$ AU. The mean value of the mass-loss rate of the dense core is $\sim 10^{-3} M_\odot \text{yr}^{-1}$, similar to that obtained by Lee et al. (2013a), which is $\sim 1.15 \times 10^{-3} M_\odot \text{yr}^{-1}$.

3. RESULTS

3.1. Model 1: Two-Bullet Model

Figure 4a shows the column density in Model 1 at 90 yr. As the two bullets are ejected into the dense core and AGB halo, they produce two collimated lobes, E1 and E2. For these two lobes, the lengths are ~ 6000 AU and the transverse widths are ~ 1000 AU, similar to the observed lengths and widths of the two major lobes, E1 and E2, of CRL 618. The column density shows that the majority of the bullet mass is still at the tips, which could be traced by the fast molecular outflows (Lee et al. 2013b).

3.2. Model 2: Five-Bullet Model

In Model 2, five bullets are ejected in two episodes, producing the five eastern lobes of CRL 618 (Fig. 4b). In the first episode, two bullets are ejected, producing lobes E1 and E2. In the second episode (~ 40 yr after the first episode), three bullets are ejected, producing lobes E3, E4, and E5. Lobe E3 has an inclination angle of -45° in the northeast, and it is the smallest lobe with a length of ~ 2200 AU, as seen in the observation. The lengths of lobes E4 and E5 are ~ 2800 AU and 2300 AU, respectively. A U-shaped cavity wall is seen at the base, consisting of swept-up material in the dense core.

3.3. Comparison with CO Observations

Since Model 2 can reproduce the structures of the five eastern lobes of CRL 618, here we choose this model to be compared with the observations. Since CO $J = 3-2$ has been observed at very high resolution of $\sim 0''.5$ and found to trace the fast molecular outflows reasonably well (Lee et al. 2013b), we calculate the CO $J = 3-2$ intensity maps and the position-velocity (PV) diagrams from Model 2 and compare them to the observations of the molecular outflows in the east of CRL 618. We use a radiative transfer code with an assumption of local thermal equilibrium (LTE) to calculate the CO emission. The x-axis is tilted toward us from the plane of the sky by 24° . The systemic velocity is -21.5 km s^{-1} , as adopted for CRL 618 in Lee et al. (2013a).

Figure 5 shows the comparison of low-velocity (LV) CO $J = 3-2$ emission between the observation and the model for the east side of CRL 618. The figures are plotted over the *HST* $H\alpha$ image of CRL 618 (Lee et al. 2013b) in order to show the relative distribution of the molecular outflows along the optical lobes. In the observation (Fig. 5a), the low-velocity emission shows a U-shaped cavity wall encompassing the two major lobes, with the northern

part around the northern edge of the E1 lobe and the southern part around the southern edge of the E2 lobe, extending away from the central source. A similar cavity wall is seen around the western lobe as well. These structures are also seen in the lower transition line of CO at $J = 2-1$ (Sánchez Contreras et al. 2004).

In the model (Fig. 5b), the low-velocity emission also shows a U-shaped cavity wall encompassing the E1 and E2 lobes, extending to $\sim 1''.7$ from the source. The emission is from the swept-up material in the dense core, which has a radius of 1500 AU ($\sim 1''.7$). Unlike the observation, however, no emission is seen extending over $\sim 1''.7$ from the source to $\sim 4''$ to the northeast. In our model, that region is within the AGB halo. Thus, in order to produce detectable emission there, the AGB halo could be denser than currently assumed in our model.

Figure 6 shows the comparison of high-velocity (HV) CO $J = 3-2$ emissions between the observation and the model. Both panels are also plotted over the *HST* images of CRL 618. In the observation (Fig. 6a), high-velocity (-183.2 to -114.1 km s $^{-1}$) emission is observed at the tips of lobes E1, E3, E4, and E5, but not observed at the tip of lobe E2. In the model, high-velocity emission, with a similar velocity range to that in the observation, is predicted to be seen at the tips of all the lobes. The velocity of the emission increases with distance, similar to that seen in the observation. Notice that the emission intensity in our model is about half of that observed and thus more bullet mass may be needed to produce more HV CO emission. The reason for no HV emission being detected at the tip of and along the southern edge of lobe E2 is unknown.

Figures 7a and 7b show the PV diagrams of the observed outflows in CO, cut along the axis of lobes E1 and E2. Figures 7c and 7d show the same PV diagrams but calculated from the model. In these diagrams, lobes E4 and E5 can also be seen. In Figures 7c and 7d, the bullets are seen at the tips of the outflows and thus are traced by the fast molecular

outflows. The diagrams also show that the velocities of the molecular outflows decrease linearly with the distance to the central source, as seen in the observations. The slope of the PV structure is roughly equal to $p/v_r = t/\tan\theta_i$, where p is the projected distance from the center, and t is the time after ejection. Therefore, different slopes are seen for the outflows in different ejection episodes. Notice that since no molecular emission is detected for lobe E2, no PV structure is detected for lobe E2 in the observation, as shown in Figure 7b.

4. DISCUSSIONS

4.1. Physical Properties of the Dense Core

In order to test our bullet models realistically, the physical parameters of the dense core are set to be close to those derived from the observations. The dense core is assumed to be toroidal, because the dense core seems to be the inner part of the expanding torus detected in the equatorial plane extending to 5000 AU from the center (Sánchez Contreras & Sahai 2004). In addition, bipolar and multipolar PPNe are often seen with dense tori at their waists (Kwok et al. 1998; Su et al. 1998; Volk et al. 2007; Sahai et al. 2008). The dense core is assumed to have a mean mass-loss rate of $\sim 10^{-3} M_{\odot} \text{ yr}^{-1}$, similar to the observed values [$\sim 0.7 \times 10^{-3} M_{\odot} \text{ yr}^{-1}$ in the outer part (Sánchez Contreras et al. 2004, with Helium added) and $1.2 \times 10^{-3} M_{\odot} \text{ yr}^{-1}$ in the inner part (Lee et al. 2013a)].

On the other hand, the density profile of the dense core is uncertain and assumed to be proportional to r^{-1} in our models for the first attempt. In the observations, the outer part of the dense core was observed with an angular resolution of $\sim 1''.1$ and thus was not resolved (Sánchez Contreras et al. 2004). The density profile there was assumed to be proportional to r^{-2} to model the observed emission. The inner part of the dense core was observed with an angular resolution of $\sim 0''.5$ and thus was also not resolved (Lee et al.

2013a). The density profile there was assumed to be proportional to r^{-3} , in order to have a constant mass-loss rate. These two density profiles are steeper than the density profile used in our models. If we used those steeper density profiles, the density in the innermost part of the dense core would be higher and thus more massive bullets would be needed to penetrate the dense core. Observations at higher angular resolution with the Atacama Large Millimeter/submillimeter Array (ALMA) are needed to resolve the dense core in order to better constrain the density profile of the dense core and thus the parameters of the bullets.

4.2. Multipolar Features: Precession or Bullet Ejections?

Precessing jet models have been used to reproduce the multipolar structures of CRL 618. However, a standard precessing jet model would produce point-symmetric multipolar lobes about the central source (Riera et al. 2014), inconsistent with the observations, which show asymmetric multipolar lobes about the central source. In order to produce the asymmetric multipolar lobes, Velázquez et al. (2014) adopted an asymmetrical jet-ejection mechanism for the precessing jet model. In this case, the morphology and the kinematics of the lobes can be in reasonable agreement with the observations. Nonetheless, the jet-ejection mechanism is complicated, requiring an alternation in the ejections of the jet from two sides of the precessing accretion disk around a binary companion.

Here, we extend the one-bullet model studied earlier in Dennis et al. (2008) and Balick et al. (2013) to the multi-directional bullet model in order to produce the multipolar lobes in CRL 618. In order to have a more realistic comparison with the observations, we also include the dense core detected recently in CRL 618 (Lee et al. 2013a) and set the physical parameters of our bullets using the fast molecular outflows recently detected in Lee et al. (2013b). As discussed earlier, our model can reproduce the morphology and the kinematics

of the multipolar lobes in the east of CRL 618 reasonably well. Since the lobes in the west are different from those in the east, a different set of bullets are needed to produce them. Notice that two episodes of bullet ejections are assumed in our model, based on the observations of fast molecular outflows in Lee et al. (2013b). However, since all the optical lobes were found to have similar dynamical ages (Balick et al. 2013), the bullets could also be ejected at the same time. Further observations are needed to determine this.

Although both of the precessing jet model and our multi-directional bullet model can produce the multiple lobes, there is an observational difference for the shock structures at the tips of the lobes between the two models. As seen in Figure 4 of Velázquez et al. (2014), the synthetic image shows that the shapes of the shocks produced by precessing jets are blunt (U-shaped). In our bullet model, on the other hand, the shapes at the tips of the lobes are sharp (V-shaped). In the observations of CRL 618, the shapes of the shocks are as sharp as those seen in our simulations.

4.3. The Origin of Bullets

The origin of the bullets is still uncertain. Dennis et al. (2008) argued that the bullets may be driven by an explosive magneto-hydrodynamic (MHD) mechanism (see Matt et al. 2006). Near the end of the AGB phase, the central star rotates very fast so that the magnetic field can be highly twisted near the central star. If the magnetic field is strong enough, the magnetic pressure force can drive a magneto-rotational explosion. Such an explosion event could produce multiple bullets simultaneously, producing the multipolar lobes of CRL 618. Further study is needed to determine if this kind of explosion can occur twice, as needed in our simulations.

Interestingly, extremely low isotope ratios of $^{12}\text{C}/^{13}\text{C}$ (~ 10) and $^{14}\text{N}/^{15}\text{N}$ (tentatively

found to be ~ 150) were found in the dense core at the center (Lee et al. 2013a). These low isotope ratios are unexpected to be seen in a C-rich dense core (Milam et al. 2009; Palmerini et al. 2011), such as that in CRL 618. As suggested in Lee et al. (2013a), these low ratios could be due to a hot CNO cycle as in a nova-like explosion. If this is the case, then the bullets could be ejected by these explosions. Theoretically, a nova requires a close binary system with the secondary being a white dwarf, and it is triggered by the accretion of hydrogen gas from the primary onto the white dwarf. The hydrogen gas can be pulled onto the surface of the white dwarf and then form an envelope massive enough to ignite the hot CNO cycles. If this is the case in CRL 618, then the center would be a binary system. This binary system in turn could produce the flattened common envelope around the center, seen as the expanding torus.

In our model, there are two episodes of bullet ejections. The first episode occurred about 90 yr ago, and the second episode occurred about 50 yr ago. Interestingly, by studying the HII region at the center, Tafuya et al. (2013) found that CRL 618 turned from a PPN into a PN at the center about 50 yr ago. Thus, it is possible that the second episode of bullet ejection is related to the formation of the HII region at the center and thus the evolutionary phase change of the central star.

5. CONCLUSIONS

With hydrodynamical simulations, we have studied the shaping mechanism of the multipolar PPN CRL 618 using a multi-directional bullet model. In our simulations, we include a spherical AGB halo with a mass-loss rate of $\sim 5.5 \times 10^{-5} M_{\odot} \text{ yr}^{-1}$ and a toroidal dense core with a mean mass-loss rate of $\sim 10^{-3} M_{\odot} \text{ yr}^{-1}$, as found in previous observations. Also, based on previous observations of fast molecular outflows in the east of the central source, we assume two episodes of bullet ejection, with the first at ~ 90 yr ago and the

second at ~ 50 yr ago, and with a total mass of $\sim 0.034 M_{\odot}$.

We find that our simulations can reproduce the morphology of the multipolar lobes in the east of CRL 618. The simulated CO emissions show the structure and the kinematics of the molecular outflows similar to those seen in the observations. At low velocity, the emission shows a similar cavity wall to that seen in the observations, surrounding the two major lobes in the east extending to $\sim 1''.7$ from the source. However, in order to produce the observed emission extending from $\sim 1''.7$ to $4''$, the AGB halo might need to be denser than that assumed here. At high velocity, the emission is distributed at the tips of all the lobes. The velocity increases with the distance, similar to that seen in the observation. Since the intensity is about half of that observed, more massive bullets might be needed.

The origin of the bullets is unknown. The ejection of these bullets could be due to magneto-rotational explosions or nova-like explosions around a binary companion. Interestingly, the more recent ejection at about 50 yr ago could be related to the formation of the HII region at the center when CRL 618 turned from a PPN into a PN.

Use of ZEUS-3D, developed by D. A. Clarke at the Institute for Computational Astrophysics (<http://www.ica.smu.ca>) with financial support from the Natural Sciences and Engineering Research Council of Canada (NSERC), is hereby acknowledged. P.-S.H, C.-F.L, and A. M acknowledge grants from the National Science Council of Taiwan (NSC 101-2119-M-001-002-MY3 and MoST 104-2119-M-001-015-MY3) and the Academia Sinica (Career Development Award). The authors acknowledge the support of the Theoretical Institute for Advanced Research in Astrophysics (TIARA) in Academia Sinica Institute of Astronomy and Astrophysics (ASIAA). P.-S.H. is grateful to Bruce Balick, Mark Morris, and Raghvendra Sahai for the valuable discussions during the PRCSA meeting.

REFERENCES

- Balick, B., Huarte-Espinosa, M., Frank, A., et al. 2013, *ApJ*, 772, 20
- Bujarrabal, V., Castro-Carrizo, A., Alcolea, J., & Sánchez Contreras, C. 2001, *A&A*, 377, 868
- Clarke, D. A. 1996, *ApJ*, 457, 291
- Clarke, D. A. 2010, *ApJS*, 187, 119
- Corradi, R. L. M., & Schwarz, H. E. 1995, *A&A*, 293, 871
- Cox, P., Huggins, P. J., Maillard, J.-P., et al. 2003, *ApJ*, 586, L87
- Dennis, T. J., Cunningham, A. J., Frank, A., et al. 2008, *ApJ*, 679, 1327
- Kwok, S., Su, K. Y. L., & Hrivnak, B. J. 1998, *ApJ*, 501, L117
- Lee, C.-F., & Sahai, R. 2003, *ApJ*, 586, 319
- Lee, C.-F., Hsu, M.-C., & Sahai, R. 2009, *ApJ*, 696, 1630
- Lee, C.-F., Yang, C.-H., Sahai, R., & Sánchez Contreras, C. 2013a, *ApJ*, 770, 153
- Lee, C.-F., Sahai, R., Sánchez Contreras, C., Huang, P.-S., & Hao Tay, J. J. 2013b, *ApJ*, 777, 37
- Matt, S., Frank, A., & Blackman, E. G. 2006, *ApJ*, 647, L45
- Milam, S. N., Woolf, N. J., & Ziurys, L. M. 2009, *ApJ*, 690, 837
- Montgomery, M. M. 2012, *ApJ*, 745, L25
- Nakashima, J., Fong, D., Hasegawa, T., et al. 2007, *AJ*, 134, 2035

- Palmerini, S., La Cognata, M., Cristallo, S., & Busso, M. 2011, *ApJ*, 729, 3
- Riera, A., Velázquez, P. F., Raga, A. C., Estalella, R., & Castrillón, A. 2014, *A&A*, 561, A145
- Sahai, R. 2001, in *Post-AGB Objects as a Phase of Stellar Evolution*, ed. R. Szczerba, & S. K. Górný (Dordrecht: Kluwer), 53
- Sahai, R., Morris, M., Sánchez Contreras, C., & Claussen, M. 2007, *AJ*, 134, 2200
- Sahai, R., Young, K., Patel, N., Sánchez Contreras, C., & Morris, M. 2008, *Ap&SS*, 313, 241
- Sánchez Contreras, C., Sahai, R., & Gil de Paz, A. 2002, *ApJ*, 578, 269
- Sánchez Contreras, C., Bujarrabal, V., Castro-Carrizo, A., Alcolea, J., & Sargent, A. 2004, *ApJ*, 617, 1142
- Sánchez Contreras, C., & Sahai, R. 2004, *ApJ*, 602, 960
- Smith, M. D., & Rosen, A. 2003, *MNRAS*, 339, 133
- Su, K. Y. L., Volk, K., Kwok, S., & Hrivnak, B. J. 1998, *ApJ*, 508, 744
- Suttner, G., Smith, M. D., Yorke, H. W., & Zinnecker, H. 1997, *A&A*, 318, 595
- Tafoya, D., Loinard, L., Fonfría, J. P., et al. 2013, *A&A*, 556, A35
- Trammell, S. R., & Goodrich, R. W. 2002, *ApJ*, 579, 688
- Velázquez, P. F., Raga, A. C., Riera, A., et al. 2012, *MNRAS*, 419, 3529
- Velázquez, P. F., Raga, A. C., Cantó, J., Schneider, E. M., & Riera, A. 2013, *MNRAS*, 428, 1587

Velázquez, P. F., Riera, A., Raga, A. C., & Toledo-Roy, J. C. 2014, 794, 128

Volk, K., Kwok, S., & Hrivnak, B. J. 2007, ApJ, 670, 1137

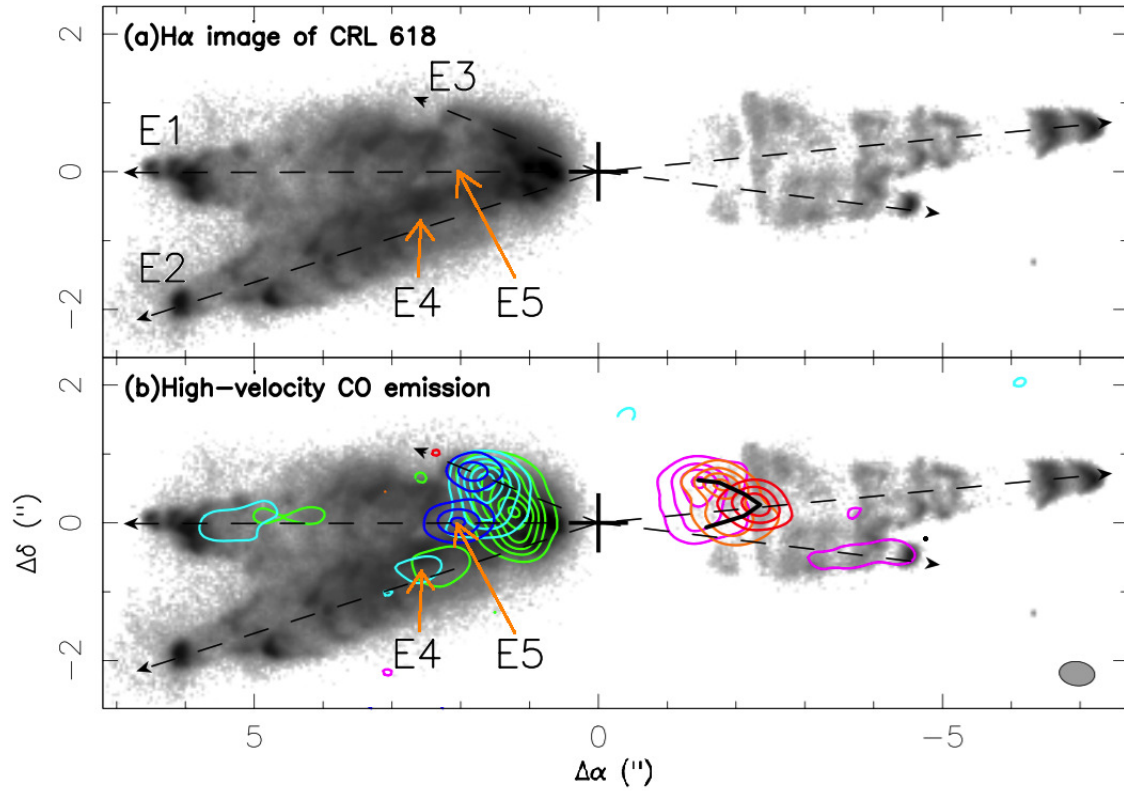


Fig. 1.— Upper panel shows the H α image of CRL 618, taken by the *HST* in 2009 August (Camera=WFC3/UVIS1, Filter=F656N, exposure time=560 s, pixel size=0".04). The eastern lobes are labeled with E1 to E5. Lobes E1, E2 and E3 are clearly detected in the H α image. Lobes E4 and E5 can not be identified in the H α image but they have been observed in the high-velocity CO emission (Lee et al. 2013b), shown in the lower panel.

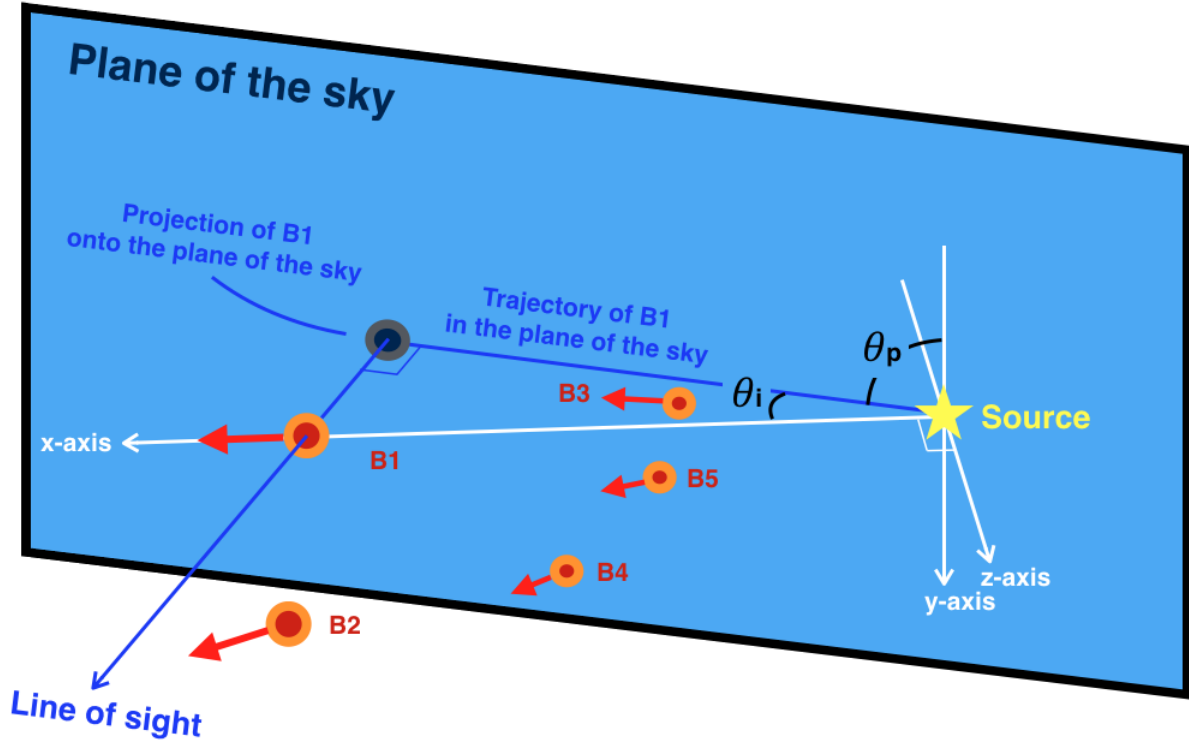


Fig. 2.— Schematic diagram of five bullets ejected from the central source. The position angles θ_p of the bullets are set to those of the optical lobes and the molecular outflows of CRL 618. The inclination angles θ_i can be obtained from the proper motions of the optical lobes (Riera et al. 2014) and the radial velocities of the molecular outflows (Lee et al. 2013b). Here we show the angles of bullet 1 (B1) as an example.

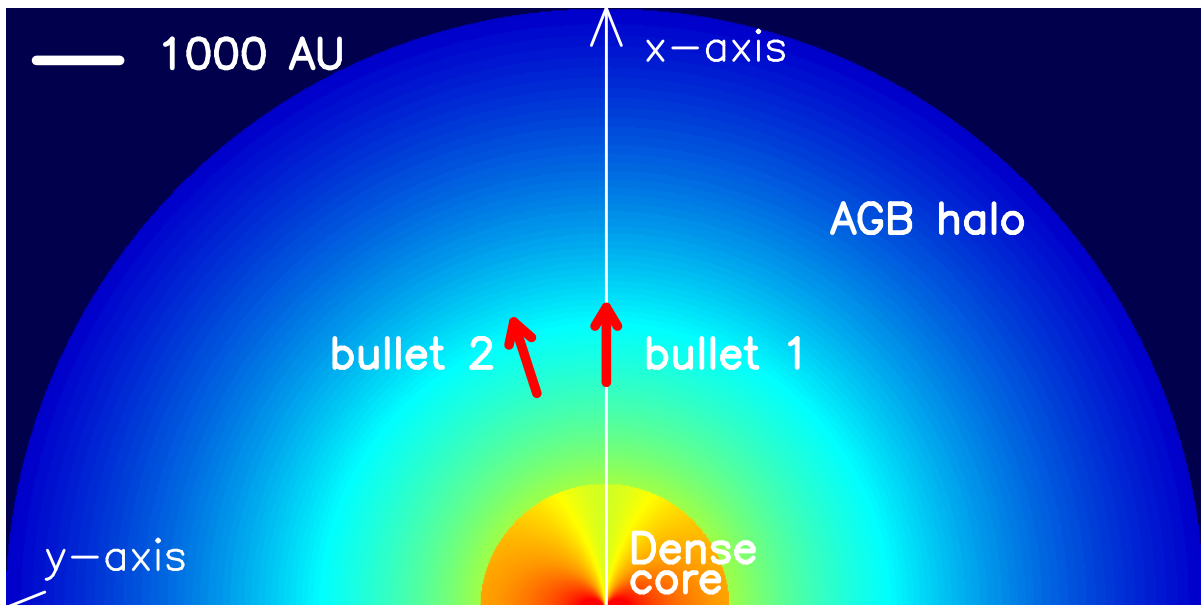


Fig. 3.— Schematic diagram of the AGB halo and the toroidal dense core, with the first two bullets. The dense core has a radius of 1500 AU.

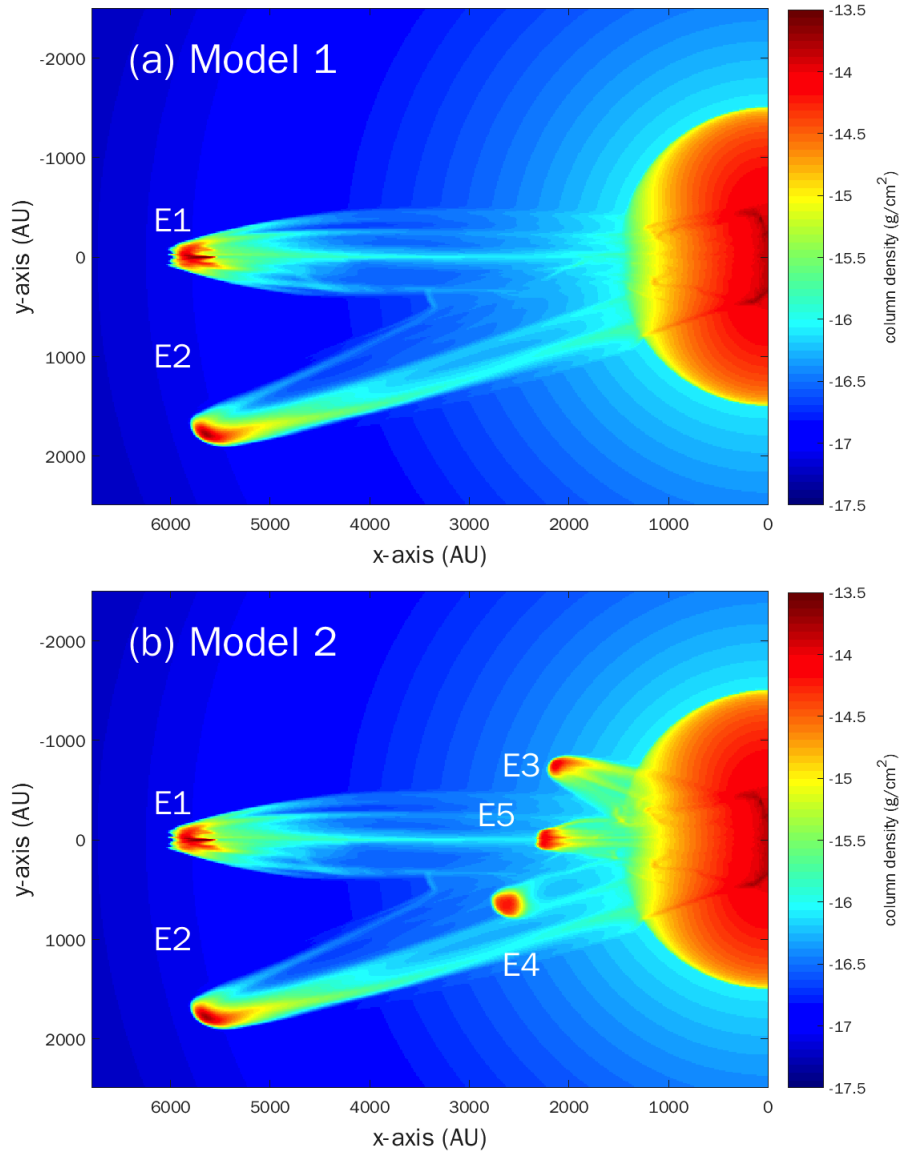


Fig. 4.— Results of ZEUS-3D simulations of (a) Model 1 and (b) Model 2. The colors show the column density, integrated along the z -axis. Panel (a) shows the result of Model 1, including the E1 (position angle of 90° , toward the east) and E2 (position angle of 108° , toward the southeast) lobes. Panel (b) shows the result of Model 2, including the E1 and E2 lobes, and also the shorter lobes E3 (toward the northeast), E4 (toward the southeast), and E5 (toward the east).

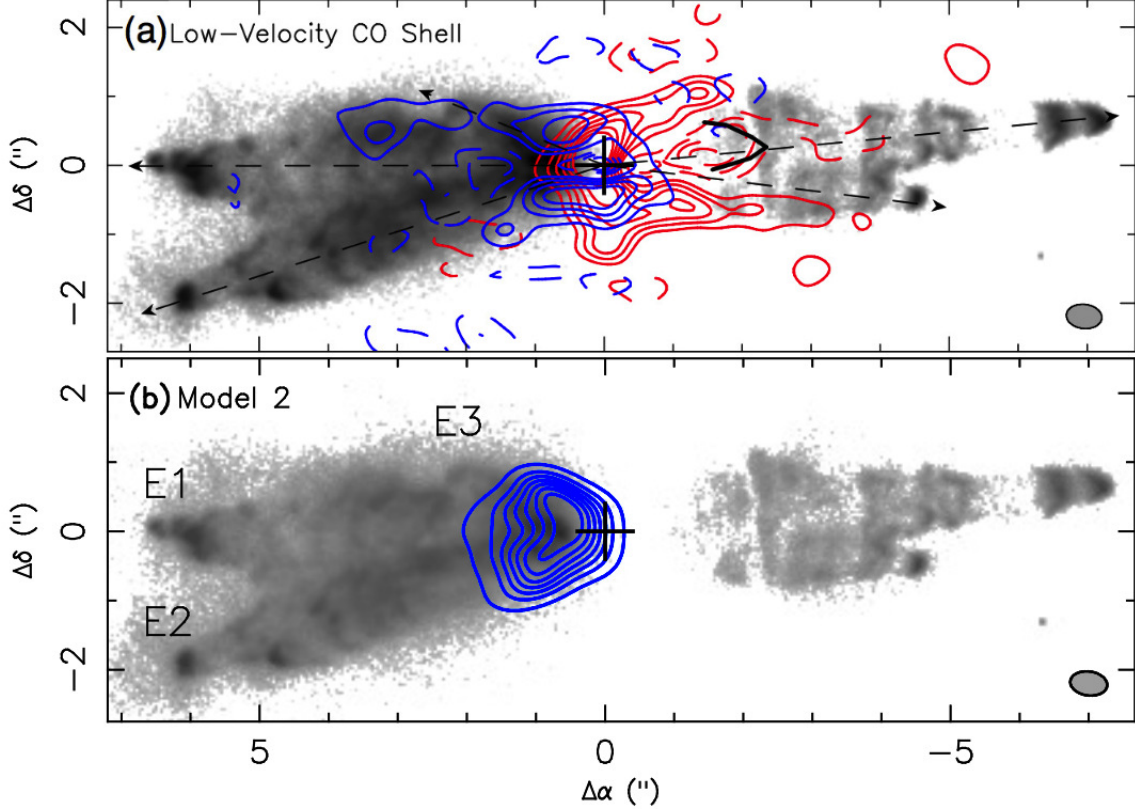


Fig. 5.— Panel (a) shows the observed low-velocity (LV) CO $J = 3-2$ emission (contours) plotted on the H α image of CRL 618 (Figure 2 of Lee et al. (2013b)). The LV CO contours show the U-shaped cavity walls in the redshifted (averaged from -16.9 to -8.5 km s $^{-1}$) and blueshifted (averaged from -35.2 to -26.8 km s $^{-1}$) emission. The systemic velocity is -21.5 km s $^{-1}$. The contour levels start at ~ 50 mJy beam $^{-1}$ with a step of ~ 100 mJy beam $^{-1}$. The synthesized beam is $\sim 0''.53 \times 0''.35$ at a position angle of $\sim 83^\circ$. Panel (b) shows the simulated CO $J = 3-2$ emission in the low velocity (averaged from -26 to -22 km s $^{-1}$), showing the cavity wall in Model 2. The contour levels and the synthesized beam are the same as in Panel (a).

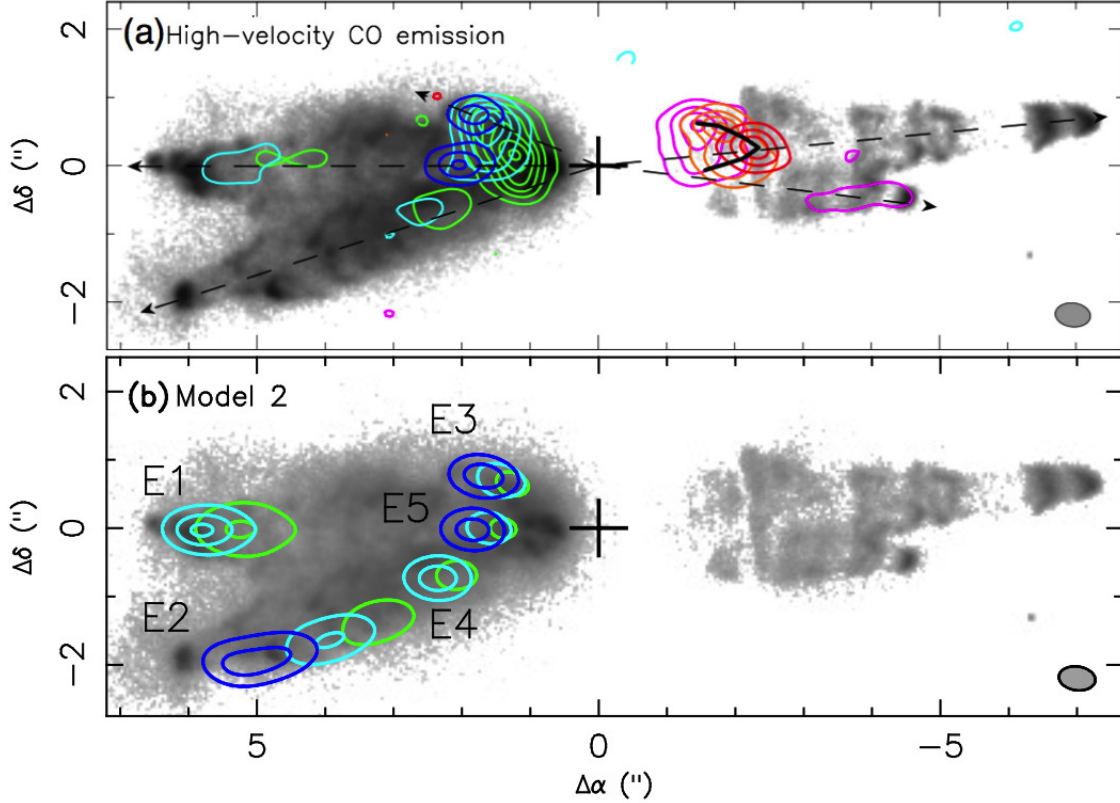


Fig. 6.— Panel (a) shows the observed high-velocity (HV) CO $J = 3-2$ emission (contours) plotted on the $H\alpha$ image of CRL 618 (from Figure 2 in Lee et al. (2013b)). The velocity ranges of the contours are: (blue) -183.2 to -160.6 , (cyan) -157.8 to -132.5 , and (green) -132.5 to -114.1 km s^{-1} . The contours start at $1 \text{ Jy beam}^{-1} \text{ km s}^{-1}$ with a step of $2 \text{ Jy beam}^{-1} \text{ km s}^{-1}$. The synthesized beam is $\sim 0''.53 \times 0''.35$ at a position angle of $\sim 83^\circ$. Panel (b) shows the simulated HV CO $J = 3-2$ emissions (contours) in Model 2, with similar velocity ranges to those in Panel (a). HV CO emissions are seen at the tips of the E1 to E5 lobes. The contours start at $0.5 \text{ Jy beam}^{-1} \text{ km s}^{-1}$ with a step of $1 \text{ Jy beam}^{-1} \text{ km s}^{-1}$. The synthesized beam is the same as that in Panel (a).

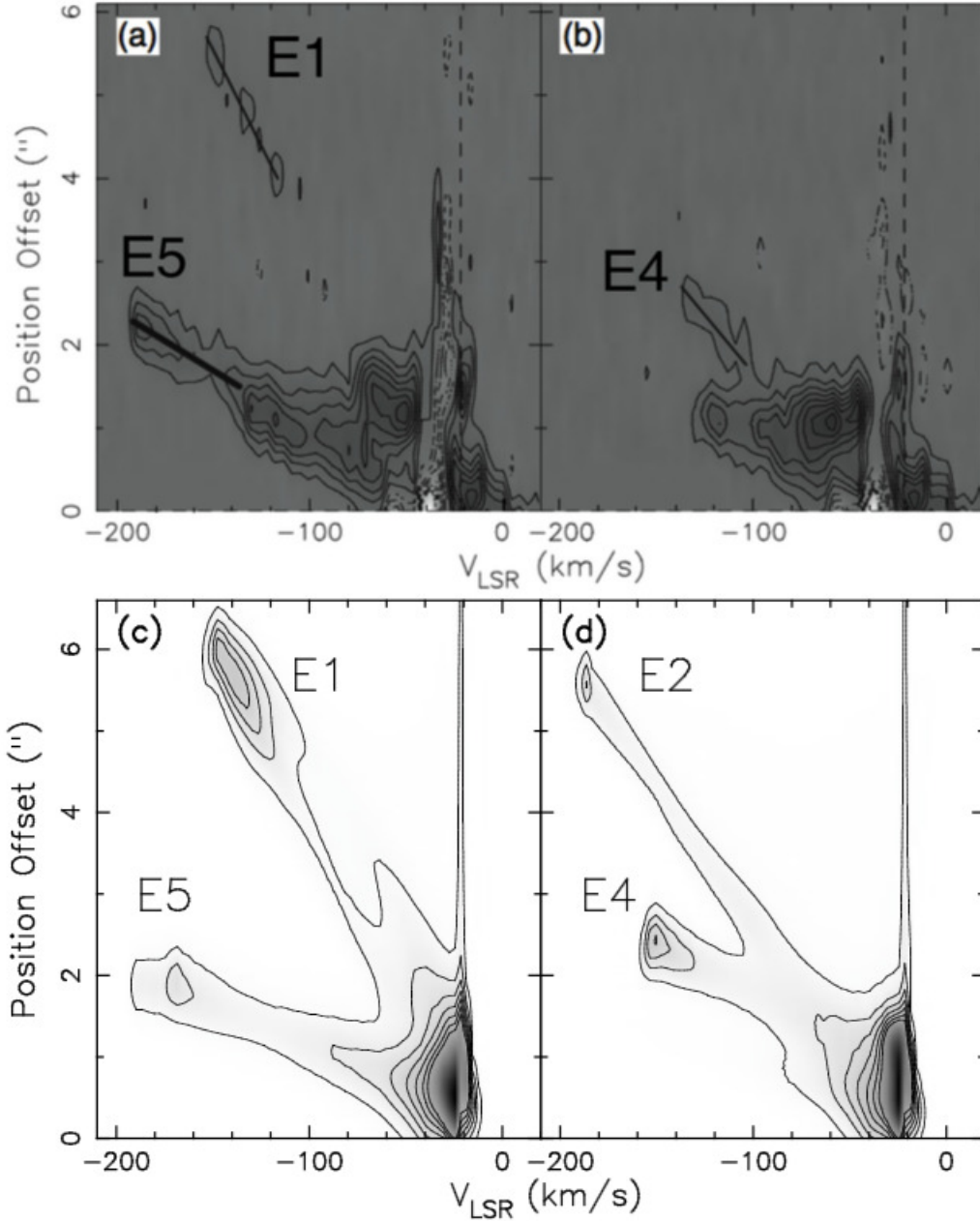


Fig. 7.— Panel (a) and (b) show the position-velocity (PV) diagrams of CO $J = 3-2$ emission of CRL 618, along the E1 and E2 lobes, respectively (from Figure 5 of Lee et al. (2013b)). The velocities linearly increase with the distance to the central source. The contours start from 40 Jy beam^{-1} with a step of 80 Jy beam^{-1} . Panel (c) and (d) shows the simulated CO emission produced by bullets 1 and 5, and bullets 2 and 4, respectively. The contours start at 20 Jy beam^{-1} with a step of 40 Jy beam^{-1} .

Table 1: Observation values of the optical lobes (^a Riera et al. 2014) and CO outflows of CRL 618 (^b Lee et al. 2013b).

Lobe	Projected length	v_t ^a (km s ⁻¹)	v_r ^b (km s ⁻¹)	$v = (v_t^2 + v_r^2)^{1/2}$ (km s ⁻¹)	θ_p	θ_i	Kinematic age (yr)
E1	6''8	288 ± 18	125	314 ± 17	90°	-24°	100
E2	6''3	243.3 ± 14	108°	...	110
E3	2''3	84 ± 18	140	163 ± 10	70°	-59°	116
E4	2''5	158 ± 18	110	193 ± 15	104°	-35°	68
E5	2''3	158 ± 18	165	228 ± 13	90°	-46°	62

Table 2: Bullet parameters in our models.

	M_b (M _⊙)	d_b (AU)	l_b (AU)	v_b (km s ⁻¹)	n_H (cm ⁻³)	θ_p	θ_i
Bullet 1	0.011	200	200	330	4.4 × 10 ⁸	90°	-24°
Bullet 2	0.011	200	200	350	4.4 × 10 ⁸	108°	-32°
Bullet 3	0.004	200	200	280	1.6 × 10 ⁸	70°	-45°
Bullet 4	0.004	200	200	240	1.6 × 10 ⁸	104°	-35°
Bullet 5	0.004	200	200	240	1.6 × 10 ⁸	90°	-45°